Photoreduction deposition preparation of UV-light-driven Pd nanoparticles/$ZnWO_4$ nanorods photocatalyst

A. Phuruangrat [a,*], Y. Chimupala [b], B. Kuntalue [c], T. Thongtem [d,e], S. Thongtem [d,f]
[a] *Division of Physical Science, Faculty of Science, Prince of Songkla University, Hat Yai, Songkhla 90112, Thailand*
[b] *Department of Industrial Chemistry, Faculty of Science, Chiang Mai University, Chiang Mai 50200, Thailand*
[c] *Advanced Scientific Instruments Unit, Faculty of Science, Chiang Mai University, Chiang Mai 50200, Thailand*
[d] *Materials Science Research Center, Faculty of Science, Chiang Mai University, Chiang Mai 50200, Thailand*
[e] *Department of Chemistry, Faculty of Science, Chiang Mai University, Chiang Mai 50200, Thailand*
[f] *Department of Physics and Materials Science, Faculty of Science, Chiang Mai University, Chiang Mai 50200, Thailand*

UV-light-driven Pd nanoparticles/$ZnWO_4$ nanorods photocatalyst was prepared by photoreduction deposition method. Effects of phase, morphology and photocatalytic properties on different weight contents of Pd loaded on $ZnWO_4$ nanorods were analyzed by XRD, SEM, TEM and XPS instruments and discussed in this research. They showed that the metallic Pd nanoparticles were uniformly decorated on the high crystalline wolframite $ZnWO_4$ nanorods. The 5% Pd/$ZnWO_4$ nanocomposites exhibited the highest rhodamine B (RhB) degradation of 92.89% within 240 min under UV light irradiation.

(Received September 15, 2024; Accepted November 14, 2024)

Keywords: $ZnWO_4$ nanorods, Metallic Pd nanoparticles, Pd−$ZnWO_4$ interfaces, Photoreduction synthesis, Photocatalysis

1. Introduction

Organic dyes released from textile, plastic and paper industries are the great impact on human health and ecological security because these organic pollutants are high stable, non-biodegradable, and likely to change genetic structure and cause cancer [1-4]. In recent years, wastewater treatment by photocatalysis has attracted very much attention and can play the role in complete transforming toxic organic compounds into CO_2 and H_2O under sun light irradiation because of the high efficiency, energy conservation, environmentally friendly and low cost process [1, 2, 5, 6].

Zinc tungsten oxide ($ZnWO_4$), an n-type semiconductor with monoclinic wolframite structure, shows excellent physicochemical properties and potential applications such as scintillating and laser host material, photocatalysis, gas detector and fiber optic device [1, 4, 7-10]. UV-light-driven $ZnWO_4$ has excellent chemical and physical stability, and good optical properties. It is low cost, environmentally friendly and nontoxic [1, 4, 11-13]. However, the UV-light-driven photocatalytic $ZnWO_4$ has low performance and high recombination rate of carrier charge pairs [1, 11-15]. One strategy for improving the UV-light-driven $ZnWO_4$ is by being loaded with noble metals because the loaded noble metals act as an electron acceptor to enhance separation of carrier charge pairs [11, 12, 16, 17]. For example, Lia et al. claimed that Ag nanocrystallites decorated on different sizes of $ZnWO_4$ nanocrystals were able to improve photodegradation of methyl orange (MO) under UV irradiation [11]. According to Zhu et al., they reported that $ZnWO_4$/Ag yolk-shell

* Corresponding author: phuruangrat@hotmail.com
https://doi.org/10.15251/DJNB.2024.194.1757

microspheres have outstanding photodegradation for methylene blue (MB) due to the hybridized Ag nanoparticles and $ZnWO_4$ nanorods [17].

In this research, Pd nanoparticles supported on surface of $ZnWO_4$ nanorods by photoreduction deposition method were reported. Weight effect of Pd nanoparticles loaded on $ZnWO_4$ nanorods used for rhodamine B (RhB) dye degradation was investigated.

2. Experiment

To prepare $ZnWO_4$ nanorods, 0.005 mole of zinc nitrate hexahydrate ($Zn(NO_3)_2 \cdot 6H_2O$) and 0.005 mole of sodium tungstate dihydrate ($Na_2WO_4 \cdot 2H_2O$) were separately dissolved in 50 ml distilled water. Following the dissolving process, the tungstate solution was slowly added to the Zn^{2+} solution to obtain white suspension. 3 M sodium hydroxide (NaOH) solution was slowly dropped to the white suspension until the suspension pH was 8. The white suspension was put in 200 ml hydrothermal reactor, tightly closed and heated at 180 °C for 24 h. The as-prepared white precipitate was separated by filtering, washed and dried for further characterization and procession.

To prepare $Pd/ZnWO_4$ nanocomposites, 2.5 g $ZnWO_4$ nanorods were added in 100 ml ethylene glycol (EG) under stirring. A certain amount of palladium (II) chloride ($PdCl_2$) was dissolved in 10 ml of EG which was slowly dropped in the $ZnWO_4$ suspension. Then, it was irradiated by UV light with stirring at 500 rpm for 3 h. The $Pd/ZnWO_4$ composites were filtered, rinsed and dried for further characterization.

To investigate UV-light-driven photocatalyst, 2.5 g photocatalyst containing in 200 ml of $1x10^{-5}$ M RhB solution as dye pollution was continuously stirred at 500 rpm for 30 min in the dark condition. Subsequently, the photocatalytic suspension was irradiated by UV light and sampled for 5 ml every 30 min interval. It was centrifuged and measured the initial and final contents of RhB at λ_{max} of 554 nm by UV-visible spectroscopy.

3. Results and discussion

Fig. 1a shows X-ray diffraction (XRD) patterns of the UV-light-driven Pd nanoparticles/$ZnWO_4$ nanorods photocatalyst. The XRD pattern of pure $ZnWO_4$ sample without the loaded Pd can be indexed to pure monoclinic $ZnWO_4$ phase according to JCPDS No. 15-0774 [18]. Strong and sharp diffraction peaks of the XRD pattern demonstrated that the sample was good crystal synthesized by hydrothermal method. The as-prepared $Pd/ZnWO_4$ heterostructure samples can be indexed to the monoclinic phase of $ZnWO_4$ as well. There was no detection the diffraction peaks of face center cubic (FCC) metallic Pd phase according to JCPDS No. 46-1043 [18] in the as-prepared $Pd/ZnWO_4$ nanocomposites because of the good dispersed crystallite of Pd nanoparticles. Fig. 1b is the Fourier transform infrared (FTIR) spectra of the as-prepared UV-light-driven Pd nanoparticles/$ZnWO_4$ nanorods photocatalyst. The stretching vibration and the asymmetric deformation of Zn−O in ZnO_6 octahedral units were detected at 431 and 472 cm^{-1}, respectively [1, 4, 5, 8, 11, 12, 16]. The FTIR bands in as-prepared samples at 888 and 821 cm^{-1} were ascribed to the Zn–O–W bending and stretching vibrations, respectively [1, 4, 8, 12, 16]. The symmetric W–O stretching in WO_6 octahedrons was detected at 728 and 573 cm^{-1} [4, 11, 12, 16]. The FTIR bands at 3200−3400 cm^{-1} of $ZnWO_4$ and $Pd/ZnWO_4$ were ascribed to the vibration of OH bond of moisture in the samples [1, 3, 5, 12, 16].

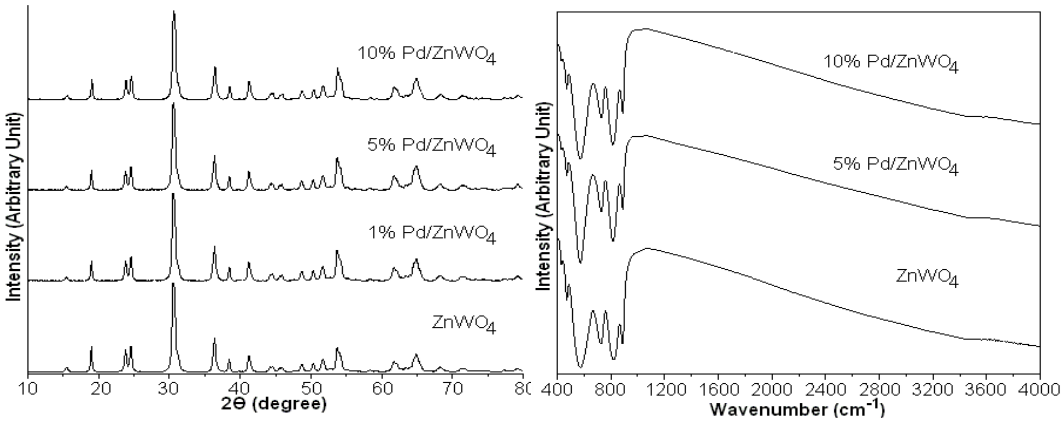

Fig. 1. (a) XRD patterns and (b) FTIR spectra of the UV-light-driven Pd nanoparticles/$ZnWO_4$ nanorods photocatalyst.

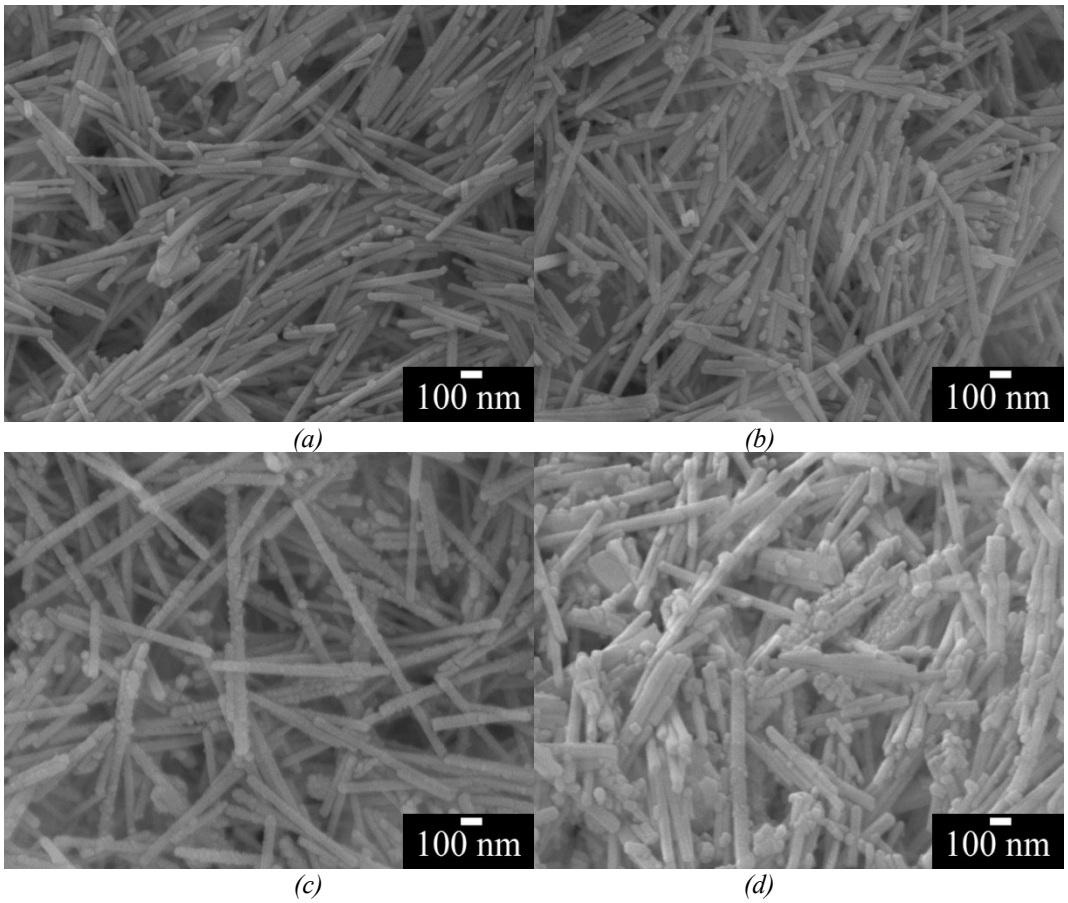

(a) *(b)*

(c) *(d)*

Fig. 2 High magnification SEM images of $ZnWO_4$ containing (a) 0%, (b) 1%, (c) 5% and (d) 10% by weight of the loaded Pd.

The morphologies of as-obtained $ZnWO_4$ samples with and without the loaded Pd were studied by scanning electron microscopy (SEM). The pure $ZnWO_4$ sample without the loaded Pd (Fig. 2a) was composed of uniform nanorods with the approximately aspect ratio of 100–150. The surface of $ZnWO_4$ nanorods was smooth. The as-obtained Pd/$ZnWO_4$ heterostructure samples are shown in Fig. 2b-d, and spherical Pd nanoparticles with <15 nm were covered on the $ZnWO_4$ surface. They certify the formation of Pd nanoparticles/$ZnWO_4$ nanorods composites.

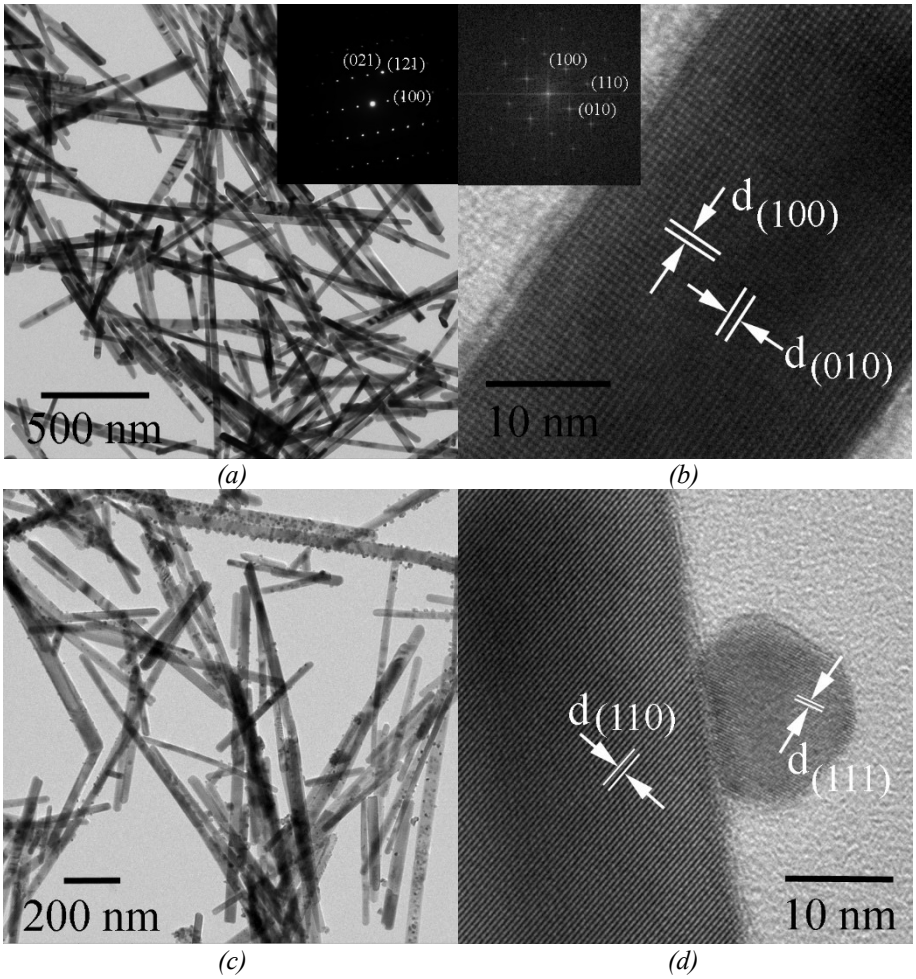

Fig. 3. TEM and HRTEM images and SAED and FFT patterns of (a, b) $ZnWO_4$ nanorods without the loaded Pd and (c, d) Pd/$ZnWO_4$ nanocomposites with 5% Pd.

Transmission electron microscopic (TEM) image of as-obtained $ZnWO_4$ sample (Fig. 3a) shows uniform nanorods with smooth surface. The SAED pattern of a single $ZnWO_4$ nanorod (inset of Fig. 3a) was indexed to the (021), (121) and (100) crystal plane of monoclinic wolframite $ZnWO_4$ structure (JCPDS No. 15-0774 [18]) with zone axis of [01–2]. HRTEM image and FFT pattern of a $ZnWO_4$ nanorod (Fig. 3b) appear as a perfect single crystal with the distinct detection of the interplanar of the (100) and (010) crystallographic planes of monoclinic $ZnWO_4$ structure (JCPDS No. 15-0774 [18]). The straight monoclinic $ZnWO_4$ nanorods preferentially grew along the [001] direction. TEM image of the as-prepared 5% Pd/$ZnWO_4$ nanocomposites (Fig. 3c) shows uniform and good distribution of spherical Pd nanoparticles on top of $ZnWO_4$ nanorods. A HRTEM image of the as-prepared 5% Pd/$ZnWO_4$ nanocomposites (Fig. 3d) shows the heterojunction of a spherical Pd nanoparticle and a $ZnWO_4$ nanorod, indicating that the heterostructure contains excellent interface. It contains the distinct interplanar of the (110) and (111) crystallographic plane of monoclinic $ZnWO_4$ structure and FCC Pd structure, confirming the formation of Pd nanoparticle–$ZnWO_4$ nanorod heterojunction by photoreduction deposition method.

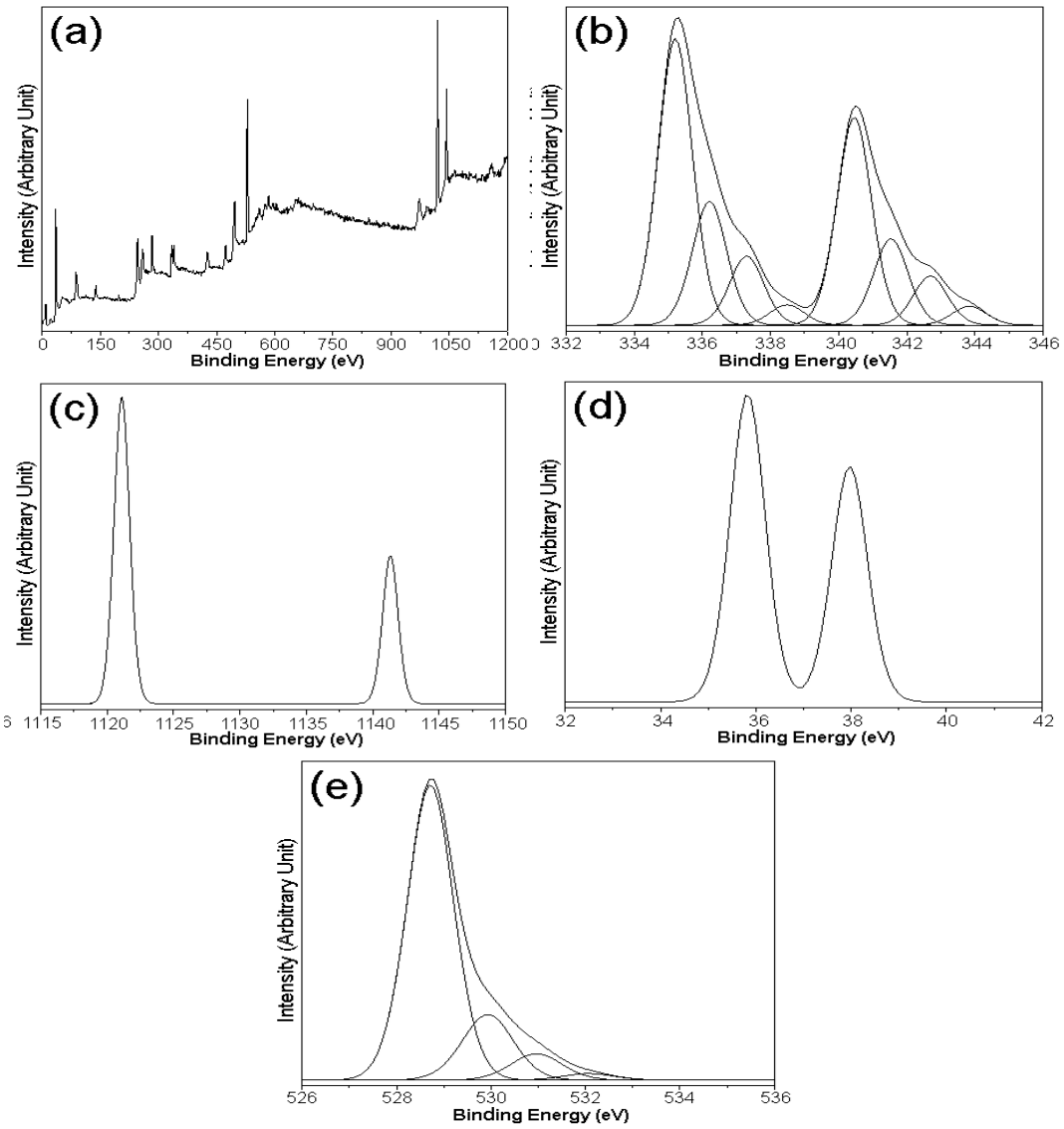

Fig. 4. (a) Survey scan XPS spectrum at 0-1200 eV and high resolution XPS binding energies peaks of (b) Pd 3d, (c) Zn 2p, (d) W 4f and (e) O 1s core levels in 5% Pd/$ZnWO_4$ nanocomposites, respectively.

The full XPS survey spectrum of as-obtained 5% Pd/$ZnWO_4$ nanocomposites (Fig. 4a) presents the only binding energies of C, Pd, Zn, W and O. The adventitious carbon element was mainly used for calibration. The high resolution XPS core levels of Pd $3d_{5/2}$ at 335.19 eV and Pd $3d_{3/2}$ at 340.44 eV were detected. They were assigned to metallic Pd^0 to which Pt^{2+} ions were reduced by photoreduction deposition method [19-21]. The energy difference of Pd 3d core levels at 336.19/337.28 and 341.52/342.67 eV for Pd $3d_{5/2}$ and Pd $3d_{3/2}$ is ascribed to Pd^{2+} of PdO and Pd^{2+} of PdO_2 containing in the as-obtained 5% Pd/$ZnWO_4$ nanocomposites [19, 21, 22]. They correspond with two peaks of palladium oxide at 338.47 and 343.82 eV [22, 23]. Zn 2p core levels of Zn^{2+} ions show two binding energies at 1021.98 and 1045.09 eV for Zn $2p_{3/2}$ and Zn $2p_{1/2}$ [12, 15, 16]. The W $4f_{7/2}$ and W $4f_{5/2}$ core levels of W^{6+} were detected at 35.83 and 37.98 eV in as-obtained 5% Pd/$ZnWO_4$ nanocomposites [12, 15, 16, 24]. The asymmetric binging energy of O 1s of as-obtained 5% Pd/$ZnWO_4$ nanocomposites was disintegrated into four symmetric binding energy peaks of O 1s at 530.71 and 531.92 eV for oxygen coordination of Zn–O bond and W–O bond of $ZnWO_4$ lattice and 532.95 and 534.06 eV for chemisorbed oxygen, including H_2O and CO_2 on the sample surface, respectively [12, 15, 16, 24]. These results show the successful formation of metallic Pd nanoparticle – $ZnWO_4$ nanorod interface.

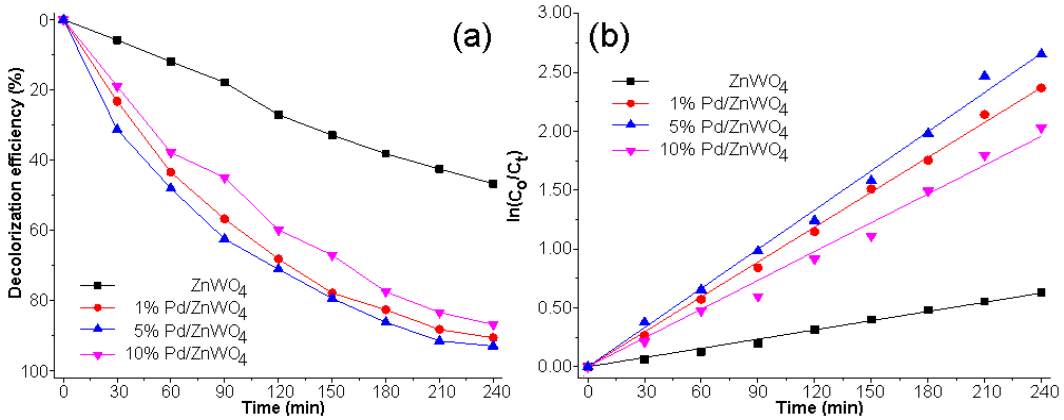

Fig. 5. (a) UV-light-driven photocatalytic efficiencies and (b) linear correlation plotted graph between the $ln(C_o/C_t)$ versus UV light irradiation time for degrading RhB over Pd nanoparticles/$ZnWO_4$ nanorods photocatalyst.

Fig. 5a shows the photocatalytic performance for RhB degradation in the presence of pure $ZnWO_4$ nanorods and heterostructure Pd/$ZnWO_4$ nanocomposites under UV light irradiation. Among them, the heterostructure 5% Pd/$ZnWO_4$ nanocomposites as UV-light-driven photocatalyst have the highest degradation because of the surface plasmon resonance (SPR) effect and electron acceptor of metallic spherical Pd nanoparticles. Fig. 5b shows the pseudo-first-order plots for photodegradation of RhB in the presence of $ZnWO_4$ nanorods and heterostructure Pd/$ZnWO_4$ nanocomposites under UV light irradiation [1, 4, 11, 12, 26, 27]. The plots of $ln(C_o/C_t)$ versus UV light irradiation time for degrading RhB in the presence of $ZnWO_4$ nanorods and heterostructure Pd/$ZnWO_4$ nanocomposites under UV light irradiation correspond with linear correlation [1, 4, 12, 27, 28]. The kinetic rate constant values for RhB degradation were $2.59x10^{-3}$, $9.88x10^{-3}$, 0.0112 and $8.16x10^{-3}$ min^{-1} for $ZnWO_4$ with weight contents of metallic spherical Pd nanoparticles of 0%, 1%, 5% and 10%, respectively.

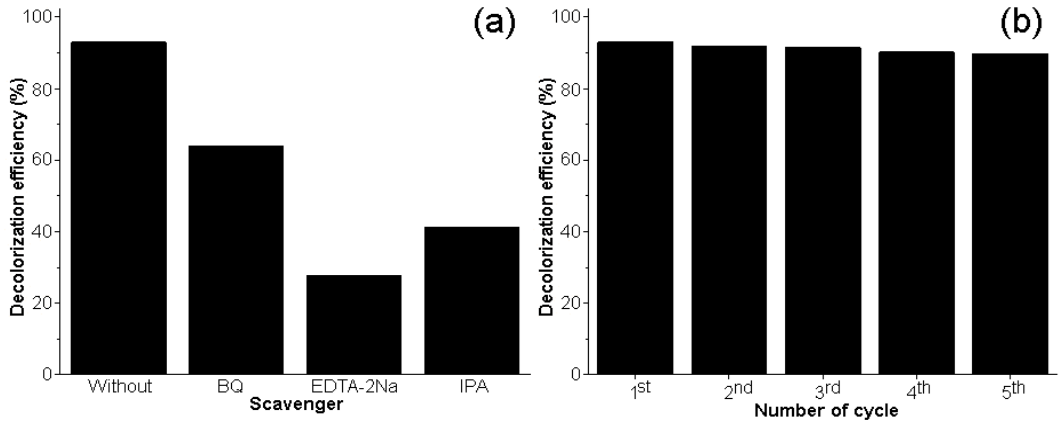

Fig. 6. (a) UV-light-driven photocatalytic efficiencies of 5% Pd/$ZnWO_4$ nanocomposites for RhB degradation with and without BQ, EDTA-2Na and IPA and (b) stability test of 5% Pd/$ZnWO_4$ nanocomposites used for photocatalysis of RhB within five recycles.

The photocatalytic performance of heterostructure 5% Pd/$ZnWO_4$ nanocomposites was 4.32 times that of $ZnWO_4$ nanorods due to the synergistic effect of Pd nanoparticles on $ZnWO_4$ nanorods. The Pd nanoparticles played the role in SPR effect to produce more photo-induced charge pairs and extend the lifetime of photo-induced charge pairs of the composites [2, 5, 11, 12, 17].

Fig. 6a shows the photodegradation efficacies of RhB over heterostructure 5% Pd/$ZnWO_4$ nanocomposites under UV light irradiation with and without different scavenger reagents. The photocatalytic efficiencies for RhB degradation were decreased from 92.98% to 63.78% for benzoquinone (BQ) for trapping of $^{\bullet}O_2^-$, 41.25% for isopropanol (IPA) for trapping of $^{\bullet}OH$ and 27.68% for ethylenediamine tetraacetic acid disodium salt (EDTA-2Na) for trapping of h^+ [3, 13, 15, 27, 29, 30]. Thus, the active species including $^{\bullet}OH$ and h^+ were very important for RhB degradation under UV light irradiation. The photo-induced charge pairs were created in valence band (VB) and conduction band (CB) on $ZnWO_4$ under UV light irradiation [2, 9, 11, 16]. Pd nanoparticles on top of $ZnWO_4$ nanorods acted as the electron acceptor at the Schottky barrier. The electrons reacted with adsorbed O_2 to generate $^{\bullet}O_2^-$ radicals, and the separation of induced charge pairs was improved [5, 9, 11, 12, 16, 17, 25]. Holes in valance band migrated to the surface of nanorods and reacted with adsorbed H_2O/OH^- to generate $^{\bullet}OH$ radicals [2, 9, 11, 16, 17]. The RhB dye was transformed into CO_2 and H_2O by active radicals. In addition, the stability of 5% Pd/$ZnWO_4$ nanocomposites was investigated for five cycles (Fig. 6b). The photocatalytic efficiency for RhB degradation over reused 5% Pd/$ZnWO_4$ nanocomposites was slightly decreased from 92.98% to 89.75% at the end of the 5th recycle. This result certifies that the heterostructure 5% Pd/$ZnWO_4$ nanocomposites are very stable for photocatalysis of dye degradation.

4. Conclusions

In this research, metallic Pd nanoparticles were successfully supported on the surface of $ZnWO_4$ nanorods by photoreduction deposition method. 5% Pd/$ZnWO_4$ nanocomposites have the highest photocatalytic efficiency for RhB degradation under UV light irradiation and are very stable in practical application for wastewater treatment.

Acknowledgements

The authors would like to thank National Science, Research and Innovation Fund (NSRF), Thailand and Prince of Songkla University under the supporting grant no. SCI6701046S.

References

[1] M. Rahmani, T. Sedaghat, Journal of Inorganic and Organometallic Polymers and Materials 29(1), 220-228 (2019); https://doi.org/10.1007/s10904-018-0981-x

[2] I. Altinsoy, N. Guy, M. Ozacar, C. Bindal, Arabian Journal for Science and Engineering 46(1), 463-4758 (2021); https://doi.org/10.1007/s13369-020-04859-y

[3] R. Wang, Z. Jiang, L. Xu, C. Liu, Journal of Materials Science: Materials in Electronics 32(6), 6931-6941 (2021); https://doi.org/10.1007/s10854-021-05399-3

[4] P.F.S. Pereira, A.F. Gouveia, M. Assis, R.C. Oliveira, I.M. Pinatti, M. Penha, R.F. Gonçalves, L. Gracia, J. Andrés, E. Longo, Physical Chemistry Chemical Physics 20(3), 1923-1937 (2018); https://doi.org/10.1039/C7CP07354B

[5] L. An, G. Wang, X. Zhou, Y. Wang, F. Gao, Y. Cheng, Russian Journal of Physical Chemistry A 88(13), 2424-2428 (2014); https://doi.org/10.1134/S003602441413010X

[6] G. Huang, Y. Zhu, CrystEngComm 14(23), 8076-8082 (2012); https://doi.org/10.1039/c2ce26005k

[7] W. Zhao, X. Song, G. Chen, S. Sun, Journal of Materials Science 44(12), 3082-3087 (2009); https://doi.org/10.1007/s10853-009-3410-2

[8] Y.X. Zhou, L. Tong, X.B. Chen, X.H. Zeng, Applied Physics A 117(2), 673-679 (2014); https://doi.org/10.1007/s00339-014-8721-8

[9] C. Zhang, H. Zhang, K. Zhang, X. Li, Q. Leng, C. Hu, ACS Applied Materials and Interfaces 6(16), 14423-14432 (2014); https://doi.org/10.1021/am503696b

[10] X. Leng, L. Dai, X. Chao, X. Yuheng, J. Xiaotian, Optik 125(3), 1267-1270 (2014) 1267-1270; https://doi.org/10.1016/j.ijleo.2013.08.033

[11] M. Li, Q. Zhu, J.G. Li, B.N. Kim, Applied Surface Science 515, 146011 (2020); https://doi.org/10.1016/j.apsusc.2020.146011

[12] P. Dumrongrojthanath, A. Phuruangrat, S. Thongtem, T. Thongtem, Rare Metals 38(7), 601-608 (2019); https://doi.org/10.1007/s12598-019-01255-w

[13] S. Mamidi, R. Gundeboina, K. Sreenu, M. Vithal, Journal of the Australian Ceramic Society 54(4), 671-678 (2018); https://doi.org/10.1007/s41779-018-0196-1

[14] O.B. Macedo, A.L.M. Oliveira, I.M.G. Santos, Ceramica 68(387), 294-315 (2022); https://doi.org/10.1590/0366-69132022683873265

[15] X. Shan, T. Jia, F. Fu, Catalysts 11(11), 1345 (2021); https://doi.org/10.3390/catal11111345

[16] C. Yu, J.C. Yu, Materials Science and Engineering: B 164(1), 16-22 (2009); https://doi.org/10.1016/j.mseb.2009.06.008

[17] J. Zhu, M. Liu, Y. Tang, T. Sun, J. Ding, L. Han, M. Wang, Materials Letters 190, 60-63 (2017); https://doi.org/10.1016/j.matlet.2016.12.056

[18] Powder Diffraction File, JCPDS-ICDD, 12 Campus Blvd, Newtown Square, PA 19073-3273, U.S.A. (2001).

[19] R.E. Priestley, A. Mansfield, J. Bye, K. Deplanche, A.B. Jorge, D. Brett, L.E. Macaskie, S. Sharma, RSC Advances 5(102), 84093-84103 (2015); https://doi.org/10.1039/C5RA12552A

[20] S. Yang, J. Dong, Z. Yao, C. Shen, X. Shi, Y. Tian, S. Lin, X. Zhang, Scientific Reports 4, 4501 (2014); https://doi.org/10.1038/srep04501

[21] Z. Li, E. Song, R. Ren, W. Zhao, T. Li, M. Liu, Y. Wu, RSC Advances 12(14), 8600-8610 (2022); https://doi.org/10.1039/D2RA00658H

[22] L.P.A. Guerrero-Ortega, E. Ramirez-Meneses, R. Cabrera-Sierra, L.M. Palacios-Romero, K. Philippot, C. R. Santiago-Ramı'rez, L. Lartundo-Rojas, A. Manzo-Robledo, Journal of Materials Science 54(21), 13694-13714 (2019); https://doi.org/10.1007/s10853-019-03843-8

[23] L.S. Kibis, A.I. Titkov, A.I. Stadnichenko, S.V. Koscheev, A.I. Boronin, Applied Surface Science 255(22), 9248-9254 (2009); https://doi.org/10.1016/j.apsusc.2009.07.011

[24] M. Claros, M. Setka, Y.P. Jimenez, S. Vallejos, Nanomaterials 10(3), 471 (2020); https://doi.org/10.3390/nano10030471

[25] H.R. Choe, S.S. Han, Y.I. Kim, C. Hong, E.J. Cho, K.M. Nam, ACS Applied Materials and Interfaces 13(1), 1714-1722 (2021); https://doi.org/10.1021/acsami.0c15488

[26] S. Wannapop, A. Inteng, R. Jareanwat, A. Somdee, Digest Journal of Nanomaterials and Biostructures 19(3), 999-1007 (2024); https://doi.org/10.15251/DJNB.2024.193.999

[27] W. J. Zeng, Y. Zhuang, M. Khan, X. T. Ning, L. F. Shan, B. Zeng, Digest Journal of Nanomaterials and Biostructures 19(3), 1107-1116 (2024); https://doi.org/10.15251/DJNB.2024.193.1107

[28] Y.T. Zhang, D.Y. Wang, X. Luo, K. Lei, L. J. Mao, Y. J. Duan, X.H. Zeng, G.J. Wan, Q. Zhao, Y. Sun, Digest Journal of Nanomaterials and Biostructures 19(2), 571-579 (2024) 79; https://doi.org/10.15251/DJNB.2024.192.571

[29] Q. Qin, L. Zhang, T. Xiao, Y.Y. Zhong, J. Wang, W.L. Liang, Y.H. Wang, S.C. Yang, X.D. Zhu, Digest Journal of Nanomaterials and Biostructures 19(2), 549-558 (2024); https://doi.org/10.15251/DJNB.2024.192.549

[30] X. Zheng, J. Yuan, J. Shen, J. Liang, J. Che, B. Tang, G. He, H. Chen, Journal of Materials Science: Materials in Electronics 30(6), 5986-5994 (2019); https://doi.org/10.1007/s10854-019-00898-w